Combustion and Flame 158 (2011) 1520–1531

Contents lists available at ScienceDirect

Combustion and Flame

journal homepage: www.elsevier.com/locate/combustflame

Spherical flame initiation and propagation with thermally sensitive intermediate kinetics

Huangwei Zhang, Zheng Chen *

State Key Laboratory for Turbulence and Complex Systems (SKLTCS), Department of Mechanics and Aerospace Engineering, College of Engineering, Peking University, Beijing 100871, China

ARTICLE INFO

Article history:
Received 7 September 2010
Received in revised form 4 November 2010
Accepted 22 December 2010
Available online 21 January 2011

Keywords:
Spherical flame initiation
Spherical flame propagation
Two-step chemistry
Lewis number
Markstein length

ABSTRACT

Spherical flame initiation and propagation with thermally sensitive intermediate kinetics are studied analytically within the framework of large activation energy and quasi-steady assumptions. A correlation describing different flame regimes and transitions among the ignition kernels, flame balls, propagating spherical flames, and planar flames is derived. Based on this correlation, spherical flame propagation and initiation are then investigated. The flame propagation speed, Markstein length, and critical ignition power and radius are found to strongly depend on the Lewis numbers of fuel and radical and the heat of reaction. For spherical flame propagation, the trajectory is shown to change significantly with the fuel Lewis number and a C-shaped solution curve of flame propagation speed as a function of flame radius is observed for large fuel Lewis numbers. The Markstein length is shown to increase/decrease monotonically with the fuel/radical Lewis number. The influence of stretch on flame propagation (i.e. the absolute value of Markstein length) is found to decrease with the heat of reaction. For spherical flame initiation, the critical ignition power and radius are shown to increase with the fuel Lewis number and to decrease with the radical Lewis number and heat of reaction. Three different flame initiation regimes are observed and discussed. Furthermore, the validity of theoretical prediction is confirmed by transient numerical simulations including thermal expansion and detailed chemistry.

1. Introduction

Flame initiation and propagation are the most fundamental problems in combustion research. Understanding flame initiation and propagation are important for fire safety control and for the development of high-efficiency, low-emission combustion engines. Since spherical flame has the simplest geometry, spherical flame initiation and propagation have been extensively studied via theoretical analysis [1–21].

Spherical flame initiation was first investigated based on the thermal theory [1–3]. The quenching distance or flame thickness was considered to be the critical length controlling spherical flame initiation. However, fuel consumption and thus mass diffusion were not considered in the thermal theory [1–3]. A more accurate description of flame initiation was proposed later by Zel'dovich based on studies of adiabatic flame balls [3]. Since the adiabatic flame balls were found to be inherently unstable: a small perturbation will cause the flame either to propagate inward and eventually extinguish or to propagate outward and evolve into a planar flame [4], the flame ball radius was considered to be the critical length controlling spherical flame initiation [3–5]. Recently, He [8] found that flame initiation for mixtures with large Lewis numbers was controlled not by the radius of stationary flame ball but by a minimum flame radius for the existence of self-sustained propagating spherical flames. Chen and coworkers [10,11] showed that spherical flame initiation was strongly affected by the fuel Lewis number as well as the radiative loss.

Spherical flame propagation has also been extensively studied by using asymptotic techniques. For examples, Frankel and Sivashinsky [12] examined the thermal expansion effect and Lewis number effect on propagating spherical flames; Chung and Law [13] conducted integral analysis for propagating spherical flames; Bechtold and coworkers [14–17] studied the hydrodynamic and thermal-diffusion instabilities and effects of radiative loss in self-extinguishing and self-wrinkling flames; Ronney and Sivashisky [18] studied the expanding spherical flames within the framework of a slowly varying flame (SVF) theory; Sung et al. [19] found that positive stretch of expanding flames promotes the onset of flame pulsation; Chen et al. [21] examined the radiative effects on spherical flame propagation speed and Markstein length.

In all the studies [4–21] mentioned above, one-step, irreversible, global reaction model was employed. The popularity of this

* Corresponding author.
E-mail addresses: zhanghwbuaa@gmail.com (H. Zhang), cz@pku.edu.cn (Z. Chen).

0010-2180/$ - see front matter © 2010 The Combustion Institute. Published by Elsevier Inc. All rights reserved.
doi:10.1016/j.combustflame.2010.12.031

model is partly due to its inherent simplicity. Nevertheless, the one-step model has led to many useful and qualitatively correct predictions for spherical flame initiation and propagation [4–21]. However, in such a one-step model the fuel is converted directly into products and heat, and thus the role of energetic active radicals is not considered [22]. In practical combustion of hydrocarbon fuels, numerous elementary reactions related to fuel and reactive intermediate species appear [23]. As such, flame initiation and propagation are not only affected by properties of fuel, but also by those of intermediate species (especially radicals involved in chain branching reactions). In order to achieve more essential understanding of flame initiation and propagation, chain branching kinetics of intermediate species should also be considered. However, inclusion of complicated chemistry requires numerical calculations and the results are lack of generality.

A relative simple generalization of the one-step model is provided by the Zel'dovich–Liñán model [3,24]. The model comprises a chain branching reaction $F+Z\rightarrow 2Z$, and a chain-breaking (or recombination) reaction $Z+Z\rightarrow 2P$, where F, Z, and P represent fuel, radical, and product, respectively. This model was used by different researchers in their studies on laminar flames [25–31]. Recently, in seeking simple analytical descriptions, Dold and coworkers [22,32–34] proposed the following simplified version of the Zel'dovich–Liñán model

$$F+Z\rightarrow 2Z:\ \ k_B=A_B\exp(-T_B/T) \tag{1a}$$

$$Z+M\rightarrow P+M:\ \ k_C=A_C \tag{1b}$$

This model involves a thermally sensitive chain branching reaction (1a) with a rate constant k_B in Arrhenius form (A_B and T_B are the frequency factor and activation temperature, respectively) and a completion reaction (1b) with a rate constant k_C which is equal to the frequency factor A_C and is independent of temperature T. Based on this model, the structure and stability of non-adiabatic flame balls and propagating planar flames were investigated [22,32–34]. The simplified Zel'dovich–Liñán model was also utilized by Gubernov and coworkers [35,36] in their studies on the kinetic characteristics of flame extinction.

In this study, we will use the simplified Zel'dovich–Liñán model given in Eq. (1) to investigate spherical flame initiation and propagation. The objectives of the present study are twofold. First, we find a general theoretical description of different flame regimes and transitions among the ignition kernels, flame balls, propagating spherical flames, and planar flames. Second, we assess the effects of fuel and radical Lewis numbers and heat of reaction on flame propagation speed, Markstein length, minimum ignition energy, and critical length controlling spherical flame initiation. Compared to the works of Dold and coworkers [22,32–34], the new development of this study is that the simplified Zel'dovich–Liñán model is used to investigate the critical ignition conditions and propagating spherical flames with positive stretch rate. The rest of the paper is organized as follows. The mathematical model is introduced in the next section. In Section 3, analytical solutions for spherical flame initiation and propagation with thermally sensitive intermediate kinetics are presented and validated in limiting cases. Moreover, the effects of fuel and radical Lewis numbers and heat of reaction on spherical flame initiation and propagation are studied. In order to confirm the validity of theoretical prediction, detailed numerical simulations are conducted in Section 4. Finally, the conclusions are presented in Section 5.

2. Mathematical model

Spherical flame initiation and propagation are studied using the classical reactive–diffusive model (constant values for density ρ, specific heat C_P, diffusion coefficients of fuel D_F and radical D_Z, thermal conductivity λ, and heat of reaction Q) [37,38]. Based on the chain branching kinetics, Eq. (1), the one-dimensional conservation equations for temperature, T, and mass fractions of fuel, YF, and radical, YZ, in a spherical coordinate are

$$\rho\frac{\partial Y_F}{\partial t}=\frac{1}{r^2}\frac{\partial}{\partial r}\left(r^2\rho D_F\frac{\partial Y_F}{\partial r}\right)-W_F\omega_B \tag{2a}$$

$$\rho\frac{\partial Y_Z}{\partial t}=\frac{1}{r^2}\frac{\partial}{\partial r}\left(r^2\rho D_Z\frac{\partial Y_Z}{\partial r}\right)+W_Z(\omega_B-\omega_C) \tag{2b}$$

$$\rho C_P\frac{\partial T}{\partial t}=\frac{1}{r^2}\frac{\partial}{\partial r}\left(r^2\lambda\frac{\partial T}{\partial r}\right)+Q\omega_C \tag{2c}$$

where t and r are time and radial coordinate respectively. The reaction rates are [32,33]

$$\omega_B=\frac{\rho Y_F}{W_F}\frac{\rho Y_Z}{W_Z}A_B\exp\left(-\frac{T_B}{T}\right),\quad \omega_C=\frac{\rho Y_Z}{W_Z}\frac{\rho}{W}A_C \tag{3}$$

where W_F and W_Z are the molecular weights of fuel and radical, respectively, and W represents the mean molecular weight.

Since the constant-density model neglects thermal expansion, there is no convective flux in the governing equations. Moreover, the effects of radiative loss on spherical flame initiation and propagation [10,21] are not considered in this study. Different from previous studies considering one-step chemistry [8,10,17], we have the additional equation, Eq. (2b), depicting the radical's production by the chain branching reaction (1a), and consumption by the recombination reaction (1b) as well as the diffusion process.

Following Dold et al. [33], we introduce the non-dimensional variables:

$$t'=\frac{t}{t_s},\quad r'=\frac{r}{r_s},\quad T'=\frac{T-T_0}{T_s},\quad Y_F'=\frac{Y_F}{Y_{F0}},\quad Y_Z'=\frac{Y_Z}{Y_{Zs}} \tag{4}$$

along with the definitions

$$t_s=\frac{r_s^2\rho C_P}{\lambda},\quad r_s^2=\frac{\lambda W}{\rho^2C_PA_C},\quad Y_{Zs}=\frac{W_ZY_{F0}}{W_F},\quad Q'=\frac{QY_{F0}}{C_PT_sW_F},$$
$$\beta=\frac{T_BT_s}{(T_0+T_s)^2},\quad \sigma=\frac{T_s}{T_0+T_s} \tag{5}$$

where T_0 and Y_{F0} are, respectively, the temperature and fuel mass fraction in the fresh mixture. The Zel'dovich number, β, defined in Eq. (5) is based on the reference temperature T_0+T_s instead of the adiabatic flame temperature [22,33]. Following Refs. [22,33], the scaling temperature, T_s, is chosen so that $\omega_B=\beta^2\omega_C$ at the temperature of T_0+T_s, i.e.

$$\frac{A_BW}{A_CW_F}Y_{F0}=\beta^2\exp\left(\frac{T_B}{T_0+T_s}\right) \tag{6}$$

It is noted that unlike the non-dimensional process in Ref. [33], the mass diffusivities of fuel and radical are not used for scaling in Eq. (5). Therefore, the Lewis numbers of fuel, $Le_F=\lambda/(\rho C_PD_F)$, and radical, $Le_Z=\lambda/(\rho C_PD_Z)$, are present in the non-dimensional governing equations, and thus the effects of Le_F and Le_Z on spherical flame initiation and propagation can be assessed in this study.

In the coordinate attached to the moving flame front, $R=R(t)$, the non-dimensional conservation equations take the following form (after dropping the primes) [8,10]

$$\frac{\partial Y_F}{\partial t}-U\frac{\partial Y_F}{\partial r}=\frac{1}{Le_F}\frac{1}{r^2}\frac{\partial}{\partial r}\left(r^2\frac{\partial Y_F}{dr}\right)-\omega \tag{7a}$$

$$\frac{\partial Y_Z}{\partial t}-U\frac{\partial Y_Z}{\partial r}=\frac{1}{Le_Z}\frac{1}{r^2}\frac{\partial}{\partial r}\left(r^2\frac{\partial Y_Z}{\partial r}\right)+\omega-Y_Z \tag{7b}$$

$$\frac{\partial T}{\partial t} - U\frac{\partial T}{\partial r} = \frac{1}{r^2}\frac{\partial}{\partial r}\left(r^2\frac{\partial T}{\partial r}\right) + QY_Z \tag{7c}$$

in which $U = dR(t)/dt$ is the flame propagation speed (which is normalized by r_s/t_s with r_s and t_s defined in Eq. (5). Since r_s/t_s is proportional to the square root of thermal diffusivity when density is assumed to be constant, the equivalent dimensional flame propagation speed does depend on the thermal diffusivity and the Lewis numbers). The non-dimensional reaction rate is [33]

$$\omega = \beta^2 Y_F Y_Z \exp\left[\beta\frac{T-1}{1+\sigma(T-1)}\right] \tag{8}$$

In this study, the impact of external energy deposition on spherical flame initiation and propagation is investigated and the ignition energy is provided as a heat flux at the center. Steady-state energy deposition is employed in order to achieve an analytical solution. As demonstrated by the numerical results in Ref. [11] and also Section 4 of this study, this simplification is adequate to gain qualitative understanding of spherical flame initiation and propagation. Therefore, the boundary conditions are:

$$r \to 0, \quad r^2\frac{\partial T}{\partial r} = -q, \quad \frac{\partial Y_F}{\partial r} = 0, \quad \frac{\partial Y_Z}{\partial r} = 0 \tag{9a}$$

$$r \to \infty, \quad T = 0, \quad Y_F = 1, \quad Y_Z = 0 \tag{9b}$$

where q is the ignition power normalized by $4\pi\lambda r_s T_s$.

In the limit of large activation energy ($\beta \to +\infty$), chemical reactions are confined at an infinitesimally thin flame sheet ($r = R$). According to the asymptotic analysis conducted by Dold and coworkers [22,33], the following conditions must hold across or at the flame front ($r = R$)

$$[Y_F] = [Y_Z] = [T] = \left[\frac{\partial T}{\partial r}\right] = \left[\frac{1}{Le_F}\frac{\partial Y_F}{\partial r} + \frac{1}{Le_Z}\frac{\partial Y_Z}{\partial r}\right] = T - 1 = Y_F\frac{\partial T}{\partial r} = 0 \tag{10}$$

where the square brackets denote the difference between the variables on the unburned and burned sides, i.e. $[f] = f(r = R^+) - f(r = R^-)$. Eq. (10) indicates the continuity of temperature, mass fractions of fuel and radical, and heat flux across the flame front [22,33]. Moreover, Eq. (10) shows that the balance of radical and fuel mass flux across the flame front is required [22,33]. Extra attention should be paid to the condition $T(r = R) = 1$. This condition corresponds to the leading order asymptotic representation of the crossover temperature in a system with radical diffusion if $\beta \to +\infty$ above which the chain branching reaction rate increases exponentially when the temperature rises, up to the point where the fuel species F is depleted completely and the chain branching is damped drastically [22,33]. Besides, the last condition in Eq. (10) indicates two possibilities regarding whether peak temperature occurs near $T = 1$ or not: if the local maximum temperature is reached at $r = R$, then fuel does not have to be depleted entirely at $r = R$ and thus fuel leakage occurs in the burned domain (this corresponds to the case $Y_F|_{r=R} \neq 0$ if $\partial T/\partial r|_{r=R} = 0$); alternatively, there is no fuel leakage across the flame front ($Y_F|_{r=R} = 0$ if $\partial T/\partial r|_{r=R} \neq 0$) [22,33]. In this study, we only consider the case without fuel leakage.

3. Theoretical analysis

The unsteady problem given by Eqs. (7–9) cannot be solved analytically. As demonstrated by transient numerical simulations considering one-step chemistry [10], it is reasonable to assume that in the coordinate attached to the flame front, the flame can be considered to propagate in a quasi-steady manner ($\partial/\partial t = 0$). The quasi-steady assumption was also used in previous studies [4,8,10,12]. After combining the quasi-steady assumption and the large activation energy assumption, the governing equations become

$$-U\frac{dY_F}{dr} = \frac{1}{Le_F}\frac{1}{r^2}\frac{d}{dr}\left(r^2\frac{dY_F}{dr}\right) \tag{11a}$$

$$-U\frac{dY_Z}{dr} = \frac{1}{Le_Z}\frac{1}{r^2}\frac{d}{dr}\left(r^2\frac{dY_Z}{dr}\right) - Y_Z \tag{11b}$$

$$-U\frac{dT}{dr} = \frac{1}{r^2}\frac{d}{dr}\left(r^2\frac{dT}{dr}\right) + QY_Z \tag{11c}$$

3.1. Analytical Solutions

Eq. (11) together with conditions given by Eqs. (9) and (10) can be solved analytically in the unburned ($r \geqslant R$) and burned ($0 \leqslant r \leqslant R$) zones, respectively. The solutions are presented directly in the following and the detailed derivation can be found in the online supplemental material. The exact solution for the mass fraction of fuel is

$$Y_F(r) = \begin{cases} 0 & \text{for } 0 \leqslant r \leqslant R \\ 1 - \int_r^\infty \xi^{-2} e^{-Le_F U\xi} d\xi \Big/ \int_R^\infty \xi^{-2} e^{-Le_F U\xi} d\xi & \text{for } r \geqslant R \end{cases} \tag{12}$$

The distribution of the radical mass fraction is given by

$$Y_Z(r) = \begin{cases} Y_{Zf} e^{[0.5(ULe_Z+k)(R-r)]} \frac{F(kr, ULe_Z/k, -ULe_Z/k)}{F(kR, ULe_Z/k, -ULe_Z/k)} & \text{for } 0 \leqslant r \leqslant R \\ Y_{Zf} e^{[0.5(ULe_Z+k)(R-r)]} \frac{G(-kr, ULe_Z/k, -ULe_Z/k)}{G(-kR, ULe_Z/k, -ULe_Z/k)} & \text{for } r \geqslant R \end{cases} \tag{13}$$

where $F(a,b,c) = \int_0^1 e^{at} t^b (1-t)^c dt$, $G(a,b,c) = \int_0^\infty e^{at} t^b (1+t)^c dt$, and $k = \sqrt{(ULe_Z)^2 + 4Le_Z}$. Y_{Zf} is the radical mass fraction at the flame front, i.e. $Y_Z(r = R) = Y_{Zf}$. According to the requirement of $[Le_F^{-1}\partial Y_F/\partial r + Le_Z^{-1}\partial Y_Z/\partial r] = 0$ at $r = R$ in Eq. (10), we have

$$Y_{Zf} = \frac{Le_Z Le_F^{-1} k^{-1} R^{-2} e^{-Le_F UR} \Big/ \int_R^\infty \xi^{-2} e^{-Le_F U\xi} d\xi}{\frac{F(kR, 1+ULe_Z/k, -ULe_Z/k)}{F(kR, ULe_Z/k, -ULe_Z/k)} + \frac{G(-kR, 1+ULe_Z/k, -ULe_Z/k)}{G(-kR, ULe_Z/k, -ULe_Z/k)}} \tag{14}$$

Using the condition $T(r = R) = 1$ in Eq. (10) and the boundary conditions in Eq. (9), the analytical solution of the temperature distribution can be obtained as

$$T(r) = \begin{cases} 1 + \int_r^R \int_0^s I(s,\xi) d\xi ds + q\int_r^R s^{-2} e^{-Us} ds & \text{for } 0 \leqslant r \leqslant R \\ \left[1 + \int_R^\infty \int_s^\infty I(s,\xi) d\xi ds\right] \frac{\int_r^\infty s^{-2} e^{-Us} ds}{\int_R^\infty s^{-2} e^{-Us} ds} & \\ \quad - \int_r^\infty \int_s^\infty I(s,\xi) d\xi ds & \text{for } r \geqslant R \end{cases} \tag{15}$$

where

$$I(s,\xi) = (\xi/s)^2 e^{-U(s-\xi)} QY_Z(\xi) \tag{16}$$

Substituting the above temperature distribution into the requirement of heat flux continuity ($[\partial T/\partial r] = 0$ at $r = R$ in Eq. (10)), we obtain the following expression describing the flame propagation speed U as a function of flame radius R

$$\int_R^\infty \int_0^s I(s,\xi) d\xi ds + q\int_R^\infty s^{-2} e^{-Us} ds = 1 \tag{17}$$

The integrals in Eq. (17) can be numerically evaluated, and accordingly the effects of fuel Lewis number (Le_F), radical Lewis number (Le_Z), and heat of reaction (Q) on spherical flame ignition and propagation can be assessed.

3.2. Validation in limiting cases

Before further analysis based on the numerical solution of Eq. (17), it is necessary to examine, in different limiting cases, whether the current model can recover results for flame balls, outwardly propagating spherical flames, and planar flames.

3.2.1. Flame ball

Adiabatic and non-adiabatic flame balls with thermally sensitive intermediate kinetics, Eq. (1), were studied by Dold et al. [33]. For the adiabatic case, the following expression for the flame ball radius, R_Z, as a function of heat of reaction, Q, and Lewis numbers of fuel, Le_F, was obtained by Dold et al. [33] (modified according to the different scaling, Eq. (5), employed in this study)

$$R_Z = \frac{Q}{Le_F}\left[R_Z - \frac{1-\exp(-2R_Z\sqrt{Le_Z})}{2\sqrt{Le_Z}}\right] \tag{18}$$

It can be shown that the above expression can be derived from Eq. (17) in the limit of $U = 0$ and $q = 0$ (without ignition power deposition). Therefore, the adiabatic flame ball solution [33] is a limiting case of the present result given by Eq. (17).

3.2.2. Outwardly propagating spherical flame

Outwardly propagating spherical flame with large flame radius was analyzed under the quasi-planar flame assumption ($R \gg 1$) for one-step chemistry [12,21,39]. Similarly, solutions considering thermally sensitive intermediate kinetics can be obtained as

$$\frac{QLe_Z^2\left(U+\frac{2}{RLe_F}\right)}{[Le_Z+U(1-Le_Z)\gamma_1][Le_Z+U(1-Le_Z)\gamma_2]} = (U+\frac{2}{R})\left[1+\frac{QLe_Z\left(U+\frac{2}{RLe_F}\right)/(\gamma_1-\gamma_2)}{Le_Z+U(1-Le_Z)\gamma_2}\right] \tag{19}$$

where $\gamma_{1,2} = [-(ULe_Z+2/R) \pm \sqrt{(ULe_Z+2/R)^2+4Le_Z}]/2$. In the online supplemental material, it is shown that the above expression gives the same results as those from Eq. (17) in the limit of $R \gg 1$ and $q = 0$. As such, the present model is valid in both limits of adiabatic flame balls and traveling spherical flames and thus can provide the relationship and transition mechanism between these two flames during the flame kernel growth.

3.2.3. Planar flame

In limit of $R \to \infty$, Eq. (19) can be further simplified as

$$\frac{QLe_Z^2}{[Le_Z+U(1-Le_Z)\lambda_1][Le_Z+U(1-Le_Z)\lambda_2]} = 1+\frac{QLe_ZU/(\lambda_1-\lambda_2)}{Le_Z+U(1-Le_Z)\lambda_2} \tag{20}$$

where $\lambda_{1,2} = [-ULe_Z \pm \sqrt{(ULe_Z)^2+4Le_Z}]/2$. Eq. (20) gives the planar flame speed, U, as a function of radical Lewis number, Le_Z, and heat of reaction, Q. It is exactly the same as that derived by Dold in the limit of zero radiative loss [22].

In view of the above discussions on three limiting cases, Eq. (17) is a general solution to describe adiabatic flame balls, propagating spherical flames, and planar flames with thermally sensitive intermediate kinetics. As will be shown later, the dynamics of flame kernel growth and the transition among different flame regimes can be predicted by this correlation. Based on Eq. (17), spherical flame propagation and initiation will be investigated in the following two sub-sections, respectively.

3.3. Spherical flame propagation with chain branching reaction

We first study spherical flame propagation without ignition power deposition at the center ($q = 0$). By solving Eq. (17) numerically at different values of Le_F, Le_Z, and Q, the effects of fuel Lewis number, radical Lewis number, and heat of reaction on spherical flame propagation can be assessed.

Figure 1a shows the results for mixtures with $Le_Z = 1.0$, $Q = 2.0$, and different fuel Lewis numbers. In Fig. 1a, solutions on the horizontal axis with $U = 0$ denote flame balls, those on the right vertical axis at $R = 10^3$ denote planar flames, and those between them represent the propagating spherical flames. It is seen that the flame ball radius increases with Le_F while the normalized planar flame speed is independent of Le_F. This is consistent with results reported in previous studies considering one-step chemistry [8,10] and chain branching kinetics [22,33]. For propagating spherical flames, the propagation speed at the same flame radius is shown to decrease with Le_F. This is due to the coupling between the flame stretch, $K = 2U/R$, and the preferential diffusion of fuel and heat [40], as demonstrated by Fig. 2b. Similar results were also reported in Ref. [11] in which one-step chemistry was considered.

Figure 1a shows that, for $Le_F = 0.3$ and $Le_F = 0.5$, the flame propagation speed first increases then slightly decreases with the flame radius. The increase of U with R is due to the transition from the purely diffusion-controlled flame ball to convection–diffusion-controlled propagating spherical flame. The decrease of U with R is due to the change of K with R and the small value of Le_F at which positive flame stretch will enhance the flame propagation (see Fig. 1b) [40]. For $Le_F = 1$, U is shown to monotonically increase with

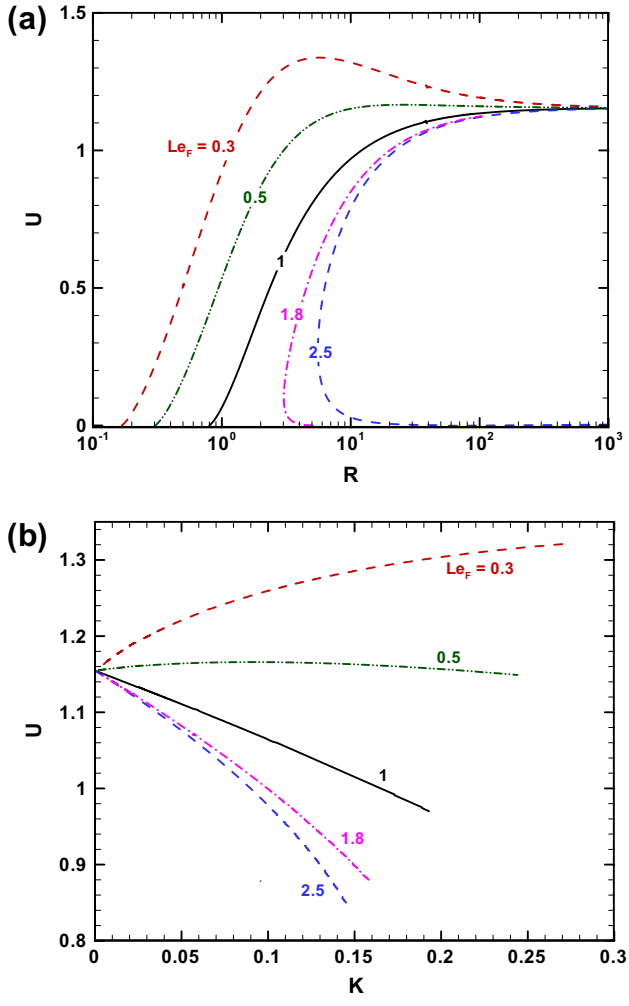

Fig. 1. Spherical flame propagation speed as a function of: (a) flame radius and (b) stretch rate for $Le_Z = 1.0$ and $Q = 2.0$.

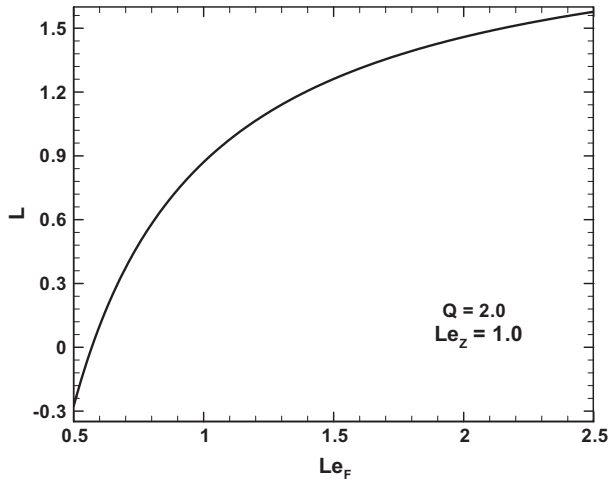

Fig. 2. Dependence of the Markstein length on the fuel Lewis number.

R. This is due to the facts shown in Fig. 1b that positive flame stretch results in slower flame propagation speed for $Le_F = 1$ and the magnitude of the stretch rate decreases during the flame propagation. At a larger Lewis number of $Le_F = 1.8$, a *C*-shaped solution curve is observed and it is seen that there exists a propagating spherical flame with radius less than the flame ball radius. This is important for spherical flame initiation discussed later since the *C*-shaped solution curve indicates that flame initiation is controlled by the minimum flame radius instead of the flame ball radius (which is commonly considered to be the minimum radius below which a spherical flame cannot propagate outwards [4,5]). Similar results were also found in studies considering one-step chemistry [8,10,11]. By further increasing the fuel Lewis number, the *C*-shaped solution curve is shifted toward the right side and there is no flame ball solution for $Le_F \geqslant 2$ and $Q = 2.0$ (according to Eq. (18), no flame ball solution exists for $Le_F \geqslant Q$). The non-existence of adiabatic flame ball at larger Lewis number is not predicted by traditional flame ball theory based on one-step chemistry [3,10,11], in which the adiabatic flame ball solution always exists for all fuel Lewis numbers.

The parameter which characterizes the variation in the local flame speed due to the influence of external stretching is the Markstein length, *L*. For weakly stretched flames ($K \ll 1$ or $R \gg 1$), there is a linear relationship between the stretched flame speed, *U*, and stretch rate, *K* [38]

$$U = U^0 - L \cdot K \tag{21}$$

where U^0 is the flame speed at zero stretch rate. Therefore, the Markstein length is equal to the slope of the *U*–*K* curve at $K \to 0$ in Fig. 1b. Figure 2 shows the dependence of the Markstein length, *L*, on the fuel Lewis number, Le_F, for $Le_Z = 1.0$ and $Q = 2.0$. It is seen that *L* increases monotonically with Le_F. For a positively stretched flame, the difference between the enthalpy gain (due to fuel diffusion into the flame) and heat loss (due to thermal conduction away from the flame) increases with Le_F since Le_F is the ratio between fuel mass diffusivity and thermal diffusivity. Therefore, the larger the fuel Lewis number, the stronger the influence of stretch on spherical flame propagation, and thus the larger the Markstein length [38,40].

In the above analysis, the radical Lewis number is fixed to be unity. The effects of radical Lewis number on spherical flame propagation are demonstrated in Fig. 3. Different flame regimes including flame balls, propagating spherical flames, and planar flames are shown in Fig. 3a. It is seen that both the flame ball radius and planar flame speed decrease with Le_Z. The same trend was also observed in previous studies on flame balls [33] and planar flames

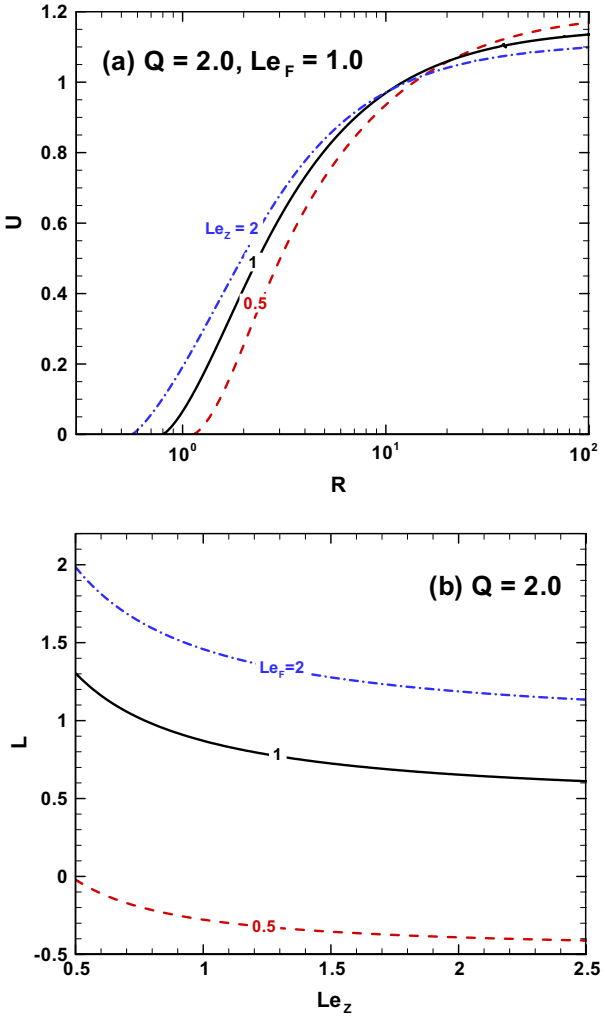

Fig. 3. Effects of radical Lewis number on: (a) flame propagation speed and (b) Markstein length.

[22] considering the same chain branching kinetics. Compared to the effects of Le_F shown in Fig. 1a, the effects of Le_Z on spherical flame propagation are shown to be much weaker since the *U*–*R* curve in Fig. 3a changes slightly with Le_Z. According to results not shown due to space limitation, the *C*-shaped *U*–*R* curve for $Le_F = 2.0$ also slightly changes with Le_Z.

The dependence of the Markstein length, *L*, on the radical Lewis number, Le_Z, are shown in Fig. 3b. Unlike the effects of Le_F shown in Fig. 2, *L* is shown to monotonically decrease with Le_Z. This is due to the fact that the radical diffuses out of the reaction zone while fuel diffuses into it. For propagating spherical flames with positive stretch, the larger the radical Lewis number, the smaller the mass diffusivity of the radical, and the less the radical enthalpy diffused away from the reaction zone. Consequently, at a given fuel Lewis number, the positively stretched flame becomes stronger for a larger radical Lewis number. Therefore, according to Eq. (21), *L* decreases with Le_Z. Comparison between Figs. 2 and 3b shows that the effects of Le_Z on *L* are also much weaker than those of Le_F.

Besides the effects of fuel and radical Lewis numbers, the effects of heat of reaction on spherical flame propagation are shown in Fig. 4. Similar to Fig. 3a, different flame regimes are shown in Fig. 4a. It is seen that the flame ball radius decreases with *Q* while the normalized planar flame speed increases with *Q*. The *U*–*R* curve is shifted toward the left side when *Q* is increased. As expected, at the same flame radius, the flame propagation speed increases with the heat of reaction. Figure 4b shows that $|L|$ always decreases with

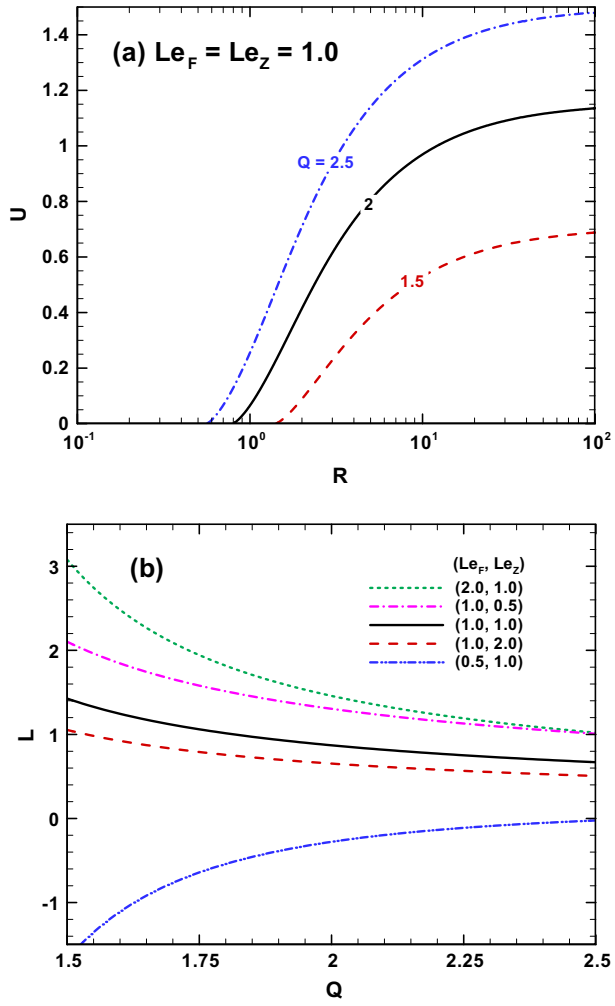

Fig. 4. Effects of heat of reaction on: (a) flame propagation speed and (b) Markstein length.

Q, indicating that the influence of stretch on flame propagation becomes weaker for a larger heat of reaction. This is because when a larger amount of heat is produced in the reaction zone, the net enthalpy gain/loss caused by preferential diffusion of various species and heat becomes relatively smaller. Accordingly, the impact of flame stretch on flame propagation becomes smaller. Therefore, weak flames are more easily affected by flame stretch than strong flames.

Summarizing, different flame regimes (flame balls, propagating spherical flames, and planar flames) and transitions among them can be successfully predicted by the present model given by Eq. (17) considering chain branching kinetics. It is shown that the spherical flame propagation speed and Markstein length are strongly affected by the Lewis numbers of fuel and radical as well as the heat of reaction.

3.4. Spherical flame initiation with chain branching reaction

We now consider cases in which an external energy flux ($q > 0$) is deposited in the center of a quiescent pre-mixture. The effects of ignition power on flame regimes and transitions among them and the critical conditions for spherical flame initiation will be examined in the following.

By solving Eq. (17) numerically, the flame propagation speed as a function of flame radius at different ignition powers can be obtained for mixtures with different values of Le_F, Le_Z, and Q. Figure 5a shows the results for $Le_F = Le_Z = 1.0$ and $Q = 2.0$. Without ignition power deposition ($q = 0$), the result is the same as that in Fig. 1a. In this case, the outwardly propagating spherical flame only exists beyond a finite flame radius, which is the flame ball radius $R_Z = 0.805$. When an external energy is deposited, the flame propagation trajectory is changed. At a low ignition power of $q = 0.14$, there exist two branches of solutions: the original traveling flame branch is shifted to the left side with the flame ball radius reduced to $R_Z^+ = 0.49$; and a new branch (ignition kernel) at small radius is formed with flame quenching occurring at the flame ball solution of $R_Z^- = 0.229$. Therefore, flame initiation fails for $q = 0.14$. With the increase of ignition power, the difference between the radii of these two flame balls, $R_Z^+ - R_Z^-$, decreases. When $R_Z^+ = R_Z^-$, occurring at $q = 0.1565$, the left ignition kernel branch merges with the right traveling flame branch, indicating that an outwardly propagating spherical flame can be successfully initiated via flame transition along the solid line shown in Fig. 5a. Therefore, for this mixture ($Le_F = Le_Z = 1.0$ and $Q = 2.0$), the critical ignition power, q_c, for successful flame initiation is determined according to the requirement of $R_Z^+ = R_Z^-$, and this flame ball radius is defined as the critical ignition radius, R_{ic} [4,5]. In the limit of $U = 0$, the general solution given by Eq. (17) reduces to

$$R_Z - \frac{Q}{Le_F}\left[R_Z + \frac{\exp\left(-2R_Z\sqrt{Le_Z}\right) - 1}{2\sqrt{Le_Z}}\right] = q \tag{22}$$

According to Eq. (22), there are two flame ball solutions, R_Z^+ and R_Z^-, for each ignition power when $Le_F = Le_Z = 1.0$, $Q = 2.0$, and $q < q_c$, as shown in Fig. 6a. At $q = q_c$, we have $R_Z^+ = R_Z^- = R_{ic}$ and thus $dq/dR_Z = 0$. Using Eq. (22), the exact solutions for q_c and R_{ic} are obtained as

$$q_c = \frac{1 + (Q/Le_F - 1)\ln(1 - Le_F/Q)}{2\sqrt{Le_Z}}, \quad R_{ic} = -\frac{\ln(1 - Le_F/Q)}{2\sqrt{Le_Z}} \tag{23}$$

Based on the above discussions, the critical conditions for spherical flame initiation, q_c and R_{ic}, can be determined by analysis on flame ball with energy deposition. This method was proposed and used by Joulin and coworkers [4,5] in their studies considering one-step chemistry. According to Eq. (23), no solutions of q_c and R_{ic} exist when $Le_F > Q$. Therefore, this analysis does not hold for mixtures with large Lewis numbers [8,10,11]. In fact, as shown in Fig. 6, there is only one flame ball solution for each ignition power when $Le_F > Q$.

Figure 5b shows results for $Le_F = 2.0$, $Le_Z = 1.0$, and $Q = 2.0$. Similar to results for $Le_F = 1.0$, there is an ignition kernel branch at small radius and a traveling flame branch at large radius for each ignition power. However, unlike the results for $Le_F = 1.0$, the traveling flame branch is C-shaped and there is no flame ball solution on it. (Though Fig. 5b shows that the traveling flame branch intersects with the R-axis at $U = 10^{-3}$, there is no intersection at $U = 0$.) Therefore, instead of flame ball radius, we use the maximum flame radius, R_C^-, on the left branch and the minimum flame radius, R_C^+, on the right branch to determine the critical ignition conditions [11]. Figure 5b shows that the points at R_C^- and R_C^+ move toward each other when the ignition power increases (as also shown in Fig. 6). When $R_C^+ = R_C^-$, the left ignition kernel branch merges with the right traveling flame branch and thus an outwardly propagating spherical flame can be successfully initiated. Therefore, the critical power for successful flame initiation is determined according to the requirement of $R_C^+ = R_C^-$, and the critical ignition radius is defined as $R_{ic} = R_C^+ = R_C^-$. The changes of R_Z^-, R_C^-, and R_C^+ with q are shown in Fig. 6a, in which (R_{ic}, q_c) is the turning point on the R_C–q curve. Similar results were found in the previous study considering one-step chemistry [11].

Figure 5c–e show the results for other different values of Le_F, Le_Z, and/or Q. Flame transitions similar to those in Fig. 5a or b

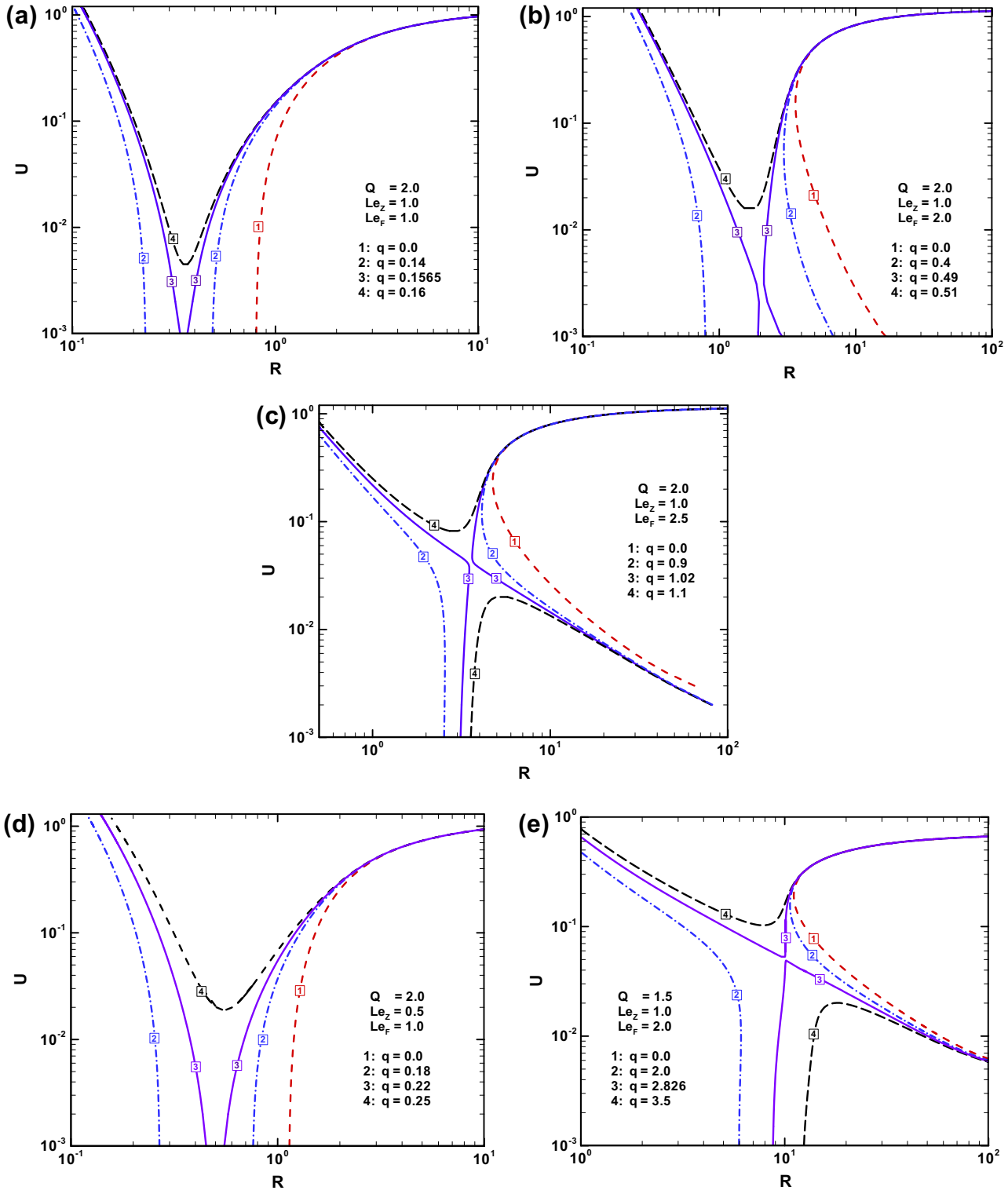

Fig. 5. Flame propagation speed as a function of flame radius at different ignition powers for mixtures with different values of Le_F, Le_Z, and Q.

are observed. The changes of the flame ball radii and the minimum and maximum flame radii with the ignition power are summarized in Fig. 6 (the upper branch represents R_C^+ or R_Z^+ and the lower one represents R_C^- or R_Z^-), in which the turning point of the R_C–q curve represents the critical ignition power and radius (R_{ic}, q_c). As mentioned before, Fig. 6 shows that the critical conditions (q_c, R_{ic}) for spherical flame initiation cannot be determined by analysis on flame ball when $Le_F > Q$. Moreover, Fig. 6 also shows that q_c and R_{ic} are affected by the Lewis numbers of fuel and radical and heat of reaction, the details of which are presented in the following.

Figure 7 shows the effects of fuel Lewis number, Le_F, on spherical flame initiation. It is seen that the critical ignition power, q_c, and the critical ignition radius, R_{ic}, both increase monotonically with Le_F. This is due to the fact that a large Le_F causes the flame

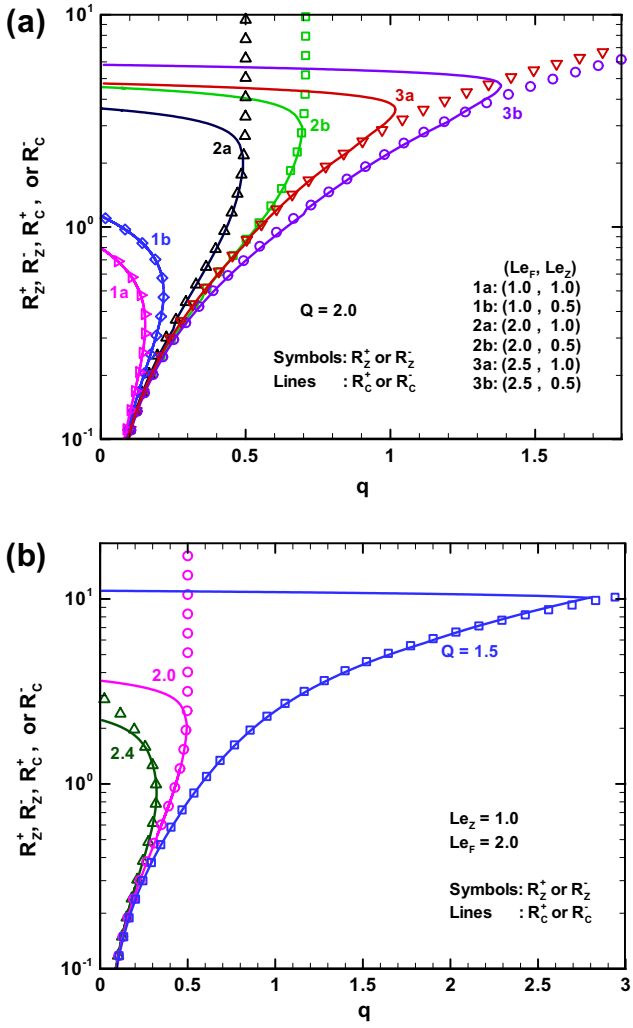

Fig. 6. Dependence of the flame ball radius (R_Z^+ and R_Z^-) and critical flame radius (R_C^+ and R_C^-) on the ignition power: (a), effects of fuel and radical Lewis numbers; (b), effects of heat of reaction. The upper branch represents R_C^+ or R_Z^+ and the lower one represents R_C^- or R_Z^-.

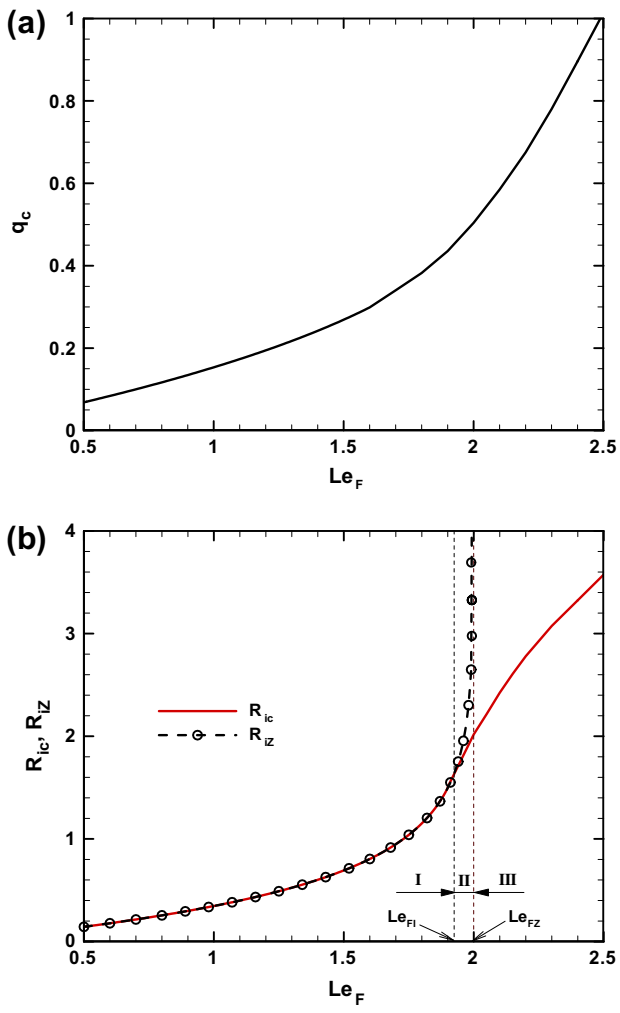

Fig. 7. Change of: (a) the critical ignition power and (b) the critical ignition radius and flame ball radius with the fuel Lewis number for $Le_Z = 1.0$ and $Q = 2.0$.

propagation speed to decrease at large stretch rate/small flame radius (see Fig. 1) and thus hinders the ignition process. The critical flame ball radius, R_{iz} (which is equal to $R_Z^+ = R_Z^-$ when $q = q_c$), is also shown in Fig. 7b for comparison. Three different regimes in terms of the fuel Lewis number are observed. In regime I with $Le_F < Le_{FI}$, we have $R_{ic} = R_{iz}$, and thus q_c and R_{ic} can be determined by Eq. (23) from flame ball analysis. In regime II with $Le_{FI} < Le_F < Le_{FZ} = Q$, we have $R_{ic} < R_{iz}$, and thus the critical ignition power will be over-predicted based on the flame ball radius. Similar results are obtained in studies considering one-step chemistry [8,10,11]. In regime III with $Le_F > Le_{FZ} = Q$, there is no critical flame ball solutions according to Eq. (23) and thus q_c and R_{ic} cannot be obtained from analysis on flame balls with energy deposition. In order to determine q_c and R_{ic}, analysis on flame propagation and transitions (see, for example, Fig. 5b) must be conducted for $Le_F > Le_{FZ}$.

The effects of radical Lewis number, Le_Z, on the critical ignition power and radius are illustrated in Fig. 8. Unlike the effects of fuel Lewis number, both q_c and R_{ic} are shown to decrease monotonically with Le_Z. This is because the Markstein length decreases with the radical Lewis number (Fig. 3b) and a large radical Lewis number causes the flame propagation speed to increase at large stretch rate/small flame radius (Fig. 3a) and thus assists the ignition process. Comparison between Figs. 7 and 8 shows that the effects of Le_Z on q_c and R_{ic} are weaker than those of Le_F. Similar comparison results are also obtained for spherical flame propagation discussed in the previous sub-section.

Figure 9 reveals the effects of heat of reaction, Q, on the critical ignition power and radius. Similar to the effects of radical Lewis number, both q_c and R_{ic} are shown to decrease monotonically with Q. It is reasonable since strong flames with larger values of Q are much easier to be initiated than weak flames with smaller values of Q. Figure 9 shows that it is extremely difficult to ignite a mixture with a large fuel Lewis number and small heat of reaction. This was confirmed by numerical simulation [11] and experiments [41,42], in which helium was added to increase the Lewis number and decrease the heat of reaction.

Figure 10 shows the three flame initiation regimes discussed above in terms of fuel Lewis number and heat of reaction. For most mixtures with fuel Lewis number close to unity, the flame initiation belongs to regime I and the critical ignition conditions, q_c and R_{ic}, can be determined by Eq. (23) from flame ball analysis. However, for mixtures with larger fuel Lewis number and/or small heat of reaction, the critical ignition power will be over-predicted based on the flame ball radius (regime II) or there is no critical flame ball solutions (regime III). In order to determine q_c and R_{ic}, analysis on flame propagation and transitions (see, for example, Fig. 5b) must be conducted in regimes II and III. The effects of radical Lewis number on these regimes are found to be negligible.

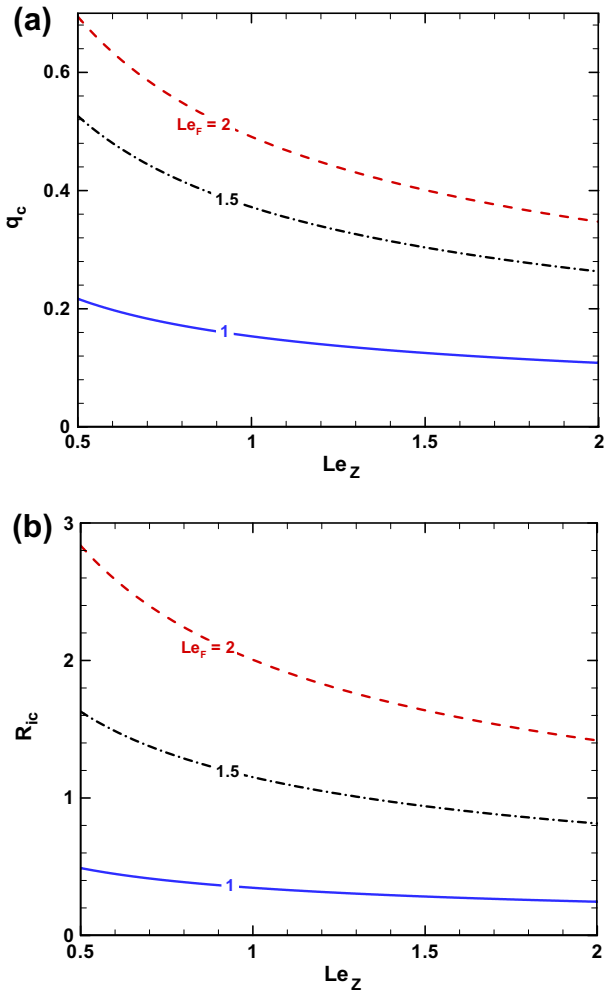

Fig. 8. Change of: (a) the critical ignition power and (b) the critical ignition radius with the radical Lewis number for $Q = 2.0$.

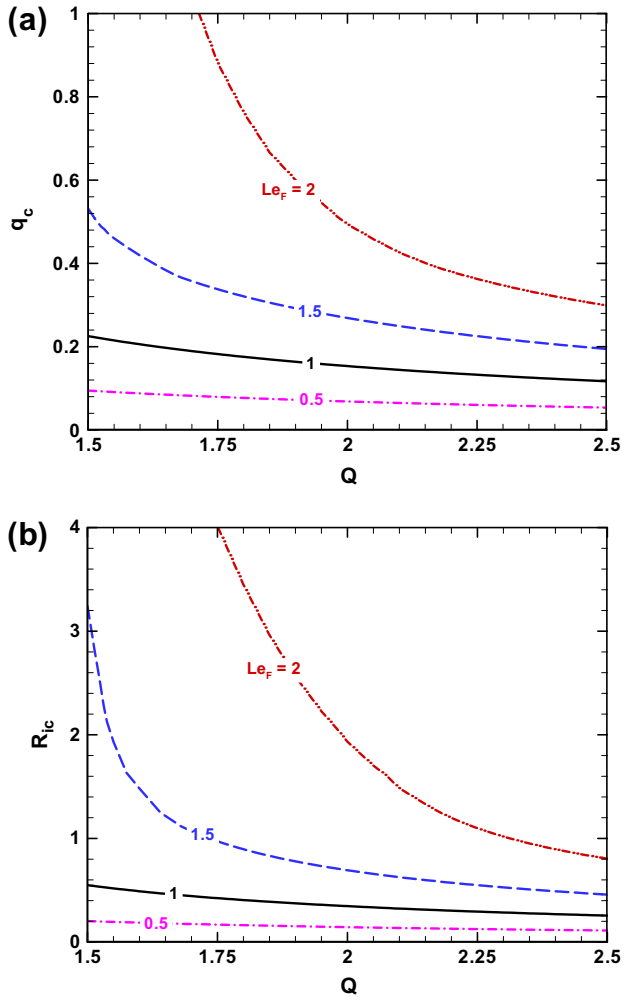

Fig. 9. Change of: (a) the critical ignition power and (b) the critical ignition radius with the heat of reaction for $Le_Z = 1.0$.

Nevertheless, the radical Lewis number does substantially affect the critical ignition power and radius (see Fig. 8).

The above results show that spherical flame initiation and propagation are strongly affected by the Lewis numbers of fuel and radical and the heat of reaction. These results are obtained from theoretical analysis. One limitation of the theory is that the ignition energy deposition is modeled as a boundary condition in the center; whereas the ignition energy addition is resolved spatially and temporally in realistic ignition systems. Moreover, the theoretical analysis is constrained by constant-density, quasi-steady, and large activation energy assumptions. In the next section, detailed numerical simulations will be conducted to test the applicability of the theoretical results under more realistic conditions. As will be shown below, the simulations qualitatively confirm the results obtained from theoretical analysis.

4. Numerical validation

A time-accurate and space-adaptive numerical solver for Adaptive Simulation of Unsteady Reactive Flow, A-SURF (1D), is used to simulate spherical flame initiation and propagation. A-SURF has been validated and used in a series of studies on spherical flame initiation and propagation [11,20,43–47]. The details on governing equations, numerical schemes, and code validation of A-SURF can be found in Refs. [20,46] and hence are only briefly described below.

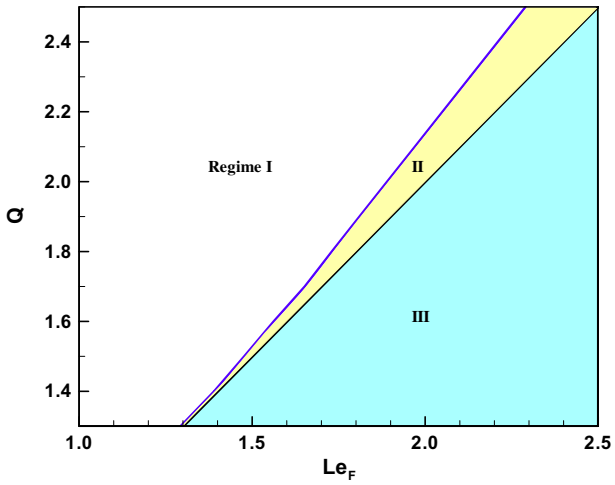

Fig. 10. Flame initiation regimes in terms of fuel Lewis number and heat of reaction for $Le_Z = 1.0$.

The one-dimensional, unsteady, compressible Navier–Stokes equations for multi-component reactive flow are solved in A-SURF. The finite volume method is used to discretize the conservation governing equations [20,46]. The convective flux, diffusive flux,

and stiff chemistry are calculated by MUSCL-Hancock scheme, central difference scheme, and VODE solver, respectively [20,46]. Detailed chemistry is considered and the reaction rates as well as thermodynamic and transport properties are evaluated using the CHEMKIN and TRANSPORT packages [48,49] interfaced with A-SURF. The mixture-averaged formula [48] is employed to calculate diffusion velocity, in which the thermal diffusion of H, H_2, and He is considered. Moreover, a correction velocity is included to ensure mass conservation [46,48].

In all the simulations, the computational domain is $0 \leqslant r \leqslant 50$ cm and a multi-level, dynamically adaptive mesh with a minimum mesh size of 8 μm is used. The flame radius, R_f, is defined as the position of maximum heat release in the simulation. Since only flames with radii less than 2.5 cm are considered, the pressure rise (<0.01%) and compression-induced flow [45,46] are negligible. Zero flow velocity and zero gradients of temperature and mass fractions are enforced at both inner ($r = 0$) and outer ($r = 50$ cm) boundaries. At the initial state, the homogeneous mixture is quiescent at 298 K and atmospheric pressure. Flame initiation is achieved by spatial dependent energy deposition for a given ignition time [11,50]

$$q_{ignit} = \begin{cases} \frac{E_{ig}}{4\pi r_{ig}^3 \tau_{ig}/3} \exp\left[-\frac{\pi}{4}\left(\frac{r}{r_{ig}}\right)^6\right] & \text{if } t < \tau_{ig} \\ 0 & \text{if } t \geqslant \tau_{ig} \end{cases} \quad (24)$$

where E_{ig} is the total ignition energy, τ_{ig}, the duration of the energy source, and r_{ig}, the ignition kernel radius. It is noted that the duration of the source energy and the ignition kernel size both affect the minimum ignition energy (MIE) [50]. In this study, since the emphasis is focused on the Lewis number effects on spherical flame initiation and propagation, both the ignition kernel size and time are kept constant with $\tau_{ig} = 200$ μs and $r_{ig} = 200$ μm, respectively.

H_2/O_2/He mixture with molar ratio of 1:1:8 is studied and the detailed chemistry developed by Li et al. [51] is employed. The fuel lean mixture is chosen due to the fact that the asymptotic analysis in Section 3 is conducted for the fuel lean case. Since the MIE of H_2/O_2/He increase significantly with the helium concentration [11], H_2/O_2 mixture highly diluted by helium instead of nitrogen is used to ensure positive Markstein length and relatively large MIE [11]. In this way, the effects of fuel and radical Lewis numbers are relatively strong according to the theoretical analysis in Section 3 and thus can be easily demonstrated in the simulation. In order to assess the effects of fuel and radical Lewis numbers on spherical flame initiation and propagation, the mass diffusivities of H_2 and H are artificially modified in the simulation. By changing the binary mass diffusion coefficient of H_2 into N_2 from D_{H_2} to $2D_{H_2}$ and $(2/3)D_{H_2}$, the fuel Lewis number becomes half and one and a half times of the original value (denoted by the superscript 0), i.e.

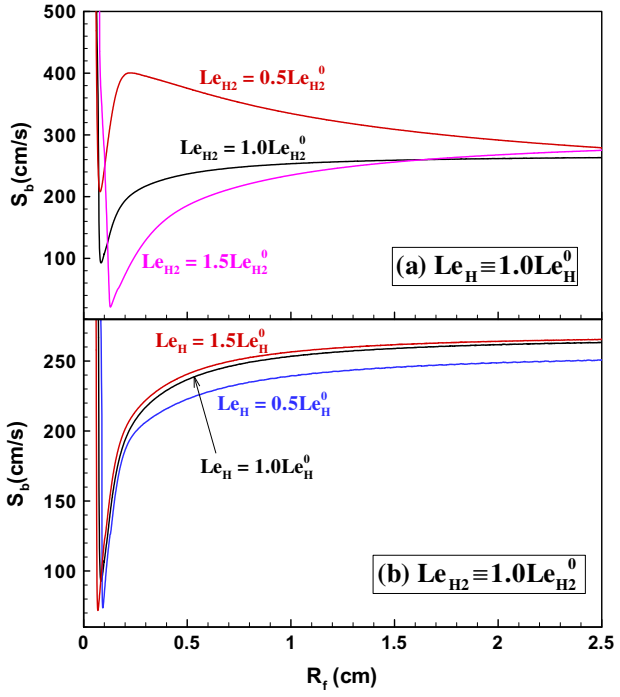

Fig. 11. Spherical flame propagation speed as a function of flame radius for H_2:O_2:He = 1:1:8 (vol.) mixture.

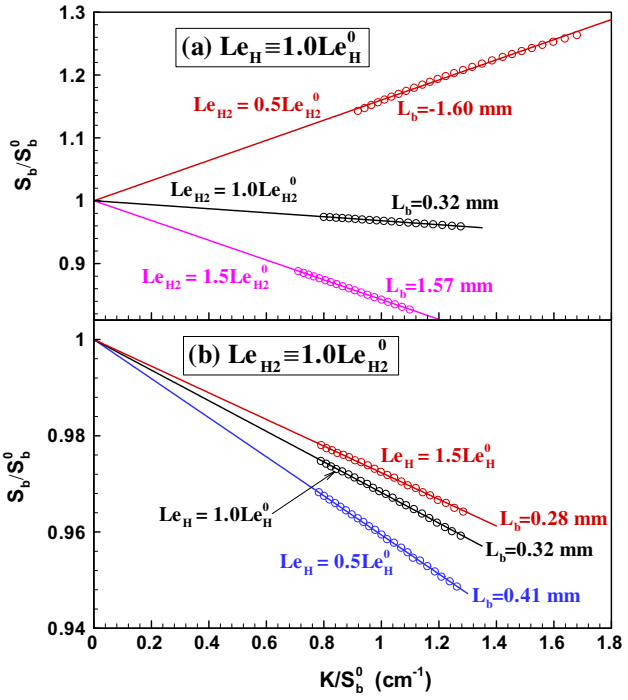

Fig. 12. Normalized spherical flame propagation speed as a function of stretch rate for H_2:O_2:He = 1:1:8 (vol.) mixture. The symbols stand for results with $1.5 \leqslant R_f \leqslant 2.5$ cm and the lines are linear extrapolations.

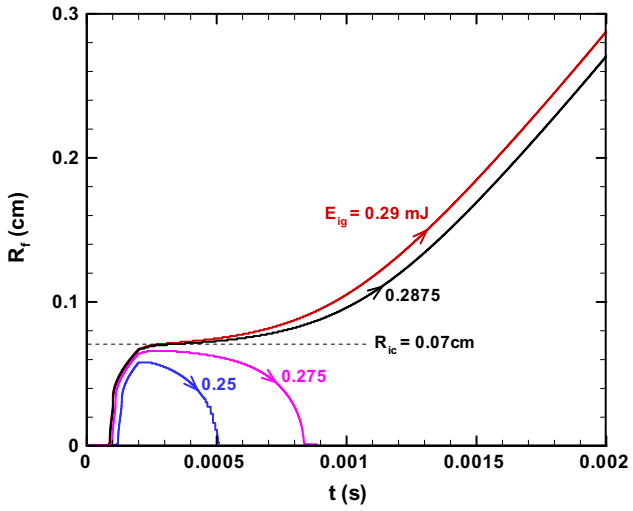

Fig. 13. Spherical flame initiation for H_2/O_2/He mixture at different ignition energies.

Table 1
The minimum ignition energies and critical ignition radii for H_2/O_2/He mixtures with different artificial Lewis numbers.

	$Le_{H_2} = 1.0Le^0_{H_2}$ $Le_H = 1.0Le^0_H$	$Le_{H_2} = 0.5Le^0_{H_2}$ $Le_H = 1.0Le^0_H$	$Le_{H_2} = 1.5Le^0_{H_2}$ $Le_H = 1.0Le^0_H$	$Le_{H_2} = 1.0Le^0_{H_2}$ $Le_H = 0.5Le^0_H$	$Le_{H_2} = 1.0Le^0_{H_2}$ $Le_H = 1.5Le^0_H$
E_{min} (mJ)	0.2875	0.2250	0.7375	0.3920	0.2475
R_{ic} (mm)	0.7	0.6	1.2	0.85	0.6

$Le_{H_2} = 0.5Le^0_{H_2}$ and $Le_{H_2} = 1.5Le^0_{H_2}$, respectively. Similarly, the radical (H is chosen because it is the most important radical in the chain branching reactions of H_2 oxidation) Lewis number can also be modified to $Le_H = 0.5Le^0_H$ and $Le_H = 1.5Le^0_H$.

Figures 11 and 12 show the effects of the fuel and radical Lewis numbers on spherical flame propagation. The propagation speed at small radius is affected by ignition and unsteadiness [20,52]. When the flame radius is large enough (say, $R_f > 6$ mm, suggested by Bradley et al. [52]), the ignition effects are negligible and the flame propagates in a quasi-steady manner. Therefore, the flame propagation speed for $R_f > 6$ mm shown in Fig. 11 is only affected by the fuel and radical Lewis numbers. When the radical Lewis number is fixed ($Le_H \equiv Le^0_H$), Fig. 11a shows the flame propagation speed is strongly affected by the fuel Lewis number. Similar to the theoretical prediction in Fig. 1a, the flame propagation speed is shown to decrease/increase with the flame radius for small/large fuel Lewis number when the flame propagates in a quasi-steady state. It is noted that the normalized planar flame speed (normalized by r_s/t_s. According to Eq. (5), r_s/t_s is approximately proportional to the square root of thermal diffusivity and thus depends the Lewis number.) is independent of the Lewis number while equivalent dimensional flame speed does increase with the fuel Lewis number. The effects of fuel Lewis number on the change of flame speed with stretch rate and the Markstein length are shown in Fig. 12a. The results are consistent with those from theoretical analysis in Fig. 1b. Similar to theoretical prediction shown in Fig. 2, the Markstein length, L_b, is found to increase with the fuel Lewis number. When the fuel Lewis number is fixed ($Le_{H_2} \equiv Le^0_{H_2}$), Fig. 11b shows that the flame propagation speed is slightly changed by the radical Lewis number, Le_H. Moreover, the Markstein length is shown (Fig. 12b) to slightly decrease with the radical Lewis number. Again, these results are consistent with theoretical prediction presented in Section 3.3.

Figure 13 shows the flame radius evolutions at different ignition energies. Neither the fuel Lewis number nor the radical Lewis number is artificially modified, i.e. $Le_{H_2} = 1.0Le^0_{H_2}$ and $Le_H = 1.0Le^0_H$. The MIE for this case, $E_{min} = 0.2875$ mJ, and for all other cases, as listed in Table 1, was calculated by the method of trial-and-error with relative error below 1%. A self-sustained propagating flame is shown to be successfully initiated only when the ignition energy is above the MIE. By plotting the flame propagating speed, $S_b = dR_f/dt$, as a function of flame radius, results similar to the theoretical predictions in Fig. 5a can be obtained. In simulation, the critical ignition radius is defined as the radius corresponding to the minimum propagating speed for MIE deposition [11,53]. According to the results in Fig. 12, the critical ignition radius, $R_{ic} = 7$ mm, occurs at the inflection point for $E = E_{min} = 0.2875$ mJ. The minimum ignition energies and critical ignition radii at different fuel and/or radical Lewis numbers are summarized in Table 1. It is seen that E_{min} and R_{ic} both increase/decrease with the fuel/radical Lewis number. These results agree qualitatively with the theoretical prediction about the effects of fuel and radical Lewis numbers on spherical flame initiation.

5. Conclusions

Spherical flame initiation and propagation are studied theoretically using the thermally sensitive intermediate kinetics, which was introduced by Dold et al. [22,33]. A correlation, Eq. (17), describing the flame propagation speed as a function of the flame radius at different fuel and radical Lewis numbers, heats of reaction, and ignition powers, is derived. It is shown to be able to describe different flame regimes and transitions among the ignition kernels, flame balls, propagating spherical flames, and planar flames. Based on this correlation, the effects of fuel and radical Lewis numbers and heat of reaction on spherical flame propagation and initiation are assessed.

Spherical flame propagation is shown to be strongly affected by the Lewis numbers of fuel and radical as well as the heat of reaction. With the increase of the fuel Lewis number, the flame propagation speed decreases due to the stretch effect. At a large fuel Lewis number, a C-shaped U–R solution curve is observed and it is found that no flame ball solution exists for $Le_F \geqslant Q$. The Markstein length is shown to increase monotonically with the fuel Lewis number. However, it decreases monotonically with the radical Lewis number since radical and fuel diffuse in the opposite directions. Compared to the effects of fuel Lewis number, these of radical Lewis number are found to be much weaker. The influence of stretch on flame propagation decreases with the heat of reaction and thus weak flames are more easily affected by flame stretch than strong flames.

The critical ignition power, q_c, and critical ignition radius, R_{ic}, for spherical flame initiation are also shown to be strongly affected by the Lewis numbers of fuel and radical as well as the heat of reaction. Both q_c and R_{ic} are shown to increase with the fuel Lewis number and to decrease with the radical Lewis number and heat of reaction. Three different regimes are observed. It is found that q_c and R_{ic} can be determined from flame ball analysis when the fuel Lewis number is small (regime I). However for mixtures with large fuel Lewis numbers or small heat of reaction (regimes II and III), analysis on flame propagation and transitions must be conducted to determine q_c and R_{ic}.

It is noted that the theory is constrained by constant-density, quasi-steady, and large activation energy assumptions. In order to confirm the validity of theoretical prediction, detailed numerical simulations are conducted to investigate the effects of fuel and radical Lewis numbers on spherical flame initiation and propagation. It is shown that the results from theoretical analysis agree qualitatively with those from numerical simulation.

Acknowledgments

This work was supported by National Natural Science Foundation of China (Grant No. 50976003) and Beijing Municipal Natural Science Foundation (Grant No. 3102016). The authors would like to thank Professor Yiguang Ju at Princeton University for his encouragement on this study.

Appendix A. Supplementary material

Supplementary data associated with this article can be found, in the online version, at doi:10.1016/j.combustflame.2010.12.031.

References

[1] B. Lewis, G. Von Elbe, Combustion Flames and Explosive of Gases, Academic Press, New York, 1961.

[2] F.A. Williams, Combustion Theory, Benjamin-Cummins, Menlo Park, CA, 1985.
[3] Y.B. Zeldovich, G.I. Barenblatt, V.B. Librovich, G.M. Makhviladze, The Mathematical Theory of Combustion and Explosions, Consultants Bureau, New York, 1985.
[4] B. Deshaies, G. Joulin, Combust. Sci. Technol. 37 (1984) 99–116.
[5] M. Champion, B. Deshaies, G. Joulin, K. Kinoshita, Combust. Flame 65 (1986) 319–337.
[6] Y. Ko, R.W. Anderson, V.S. Arpaci, Combust. Flame 83 (1991) 75–87.
[7] P.D. Ronney, Opt. Eng. 33 (1994) 510–521.
[8] L.T. He, Combust. Theor. Model. 4 (2000) 159–172.
[9] C. Vazquez-Espi, A. Linan, Combust. Theor. Model. 6 (2002) 297–315.
[10] Z. Chen, Y. Ju, Combust. Theor. Model. 11 (2007) 427–453.
[11] Z. Chen, M.P. Burke, Y. Ju, Proc. Combust. Inst. 33 (2011) 1219–1226.
[12] M.L. Frankel, G.I. Sivashinsky, Combust. Sci. Technol. 31 (1983) 131–138.
[13] S.H. Chung, C.K. Law, Combust. Flame 72 (1988) 325–336.
[14] J.K. Bechtold, M. Matalon, Combust. Flame 67 (1987) 77–90.
[15] R. Addabbo, J.K. Bechtold, M. Matalon, Proc. Combust. Inst. 29 (2003) 1527–1535.
[16] M. Matalon, C. Cui, J.K. Bechtold, J. Fluid Mech. 487 (2003) 179–210.
[17] J.K. Bechtold, C. Cui, M. Matalon, Proc. Combust. Inst. 30 (2005) 177–184.
[18] P.D. Ronney, G.I. Sivashinsky, SIAM J. Appl. Math. 49 (1989) 1029–1046.
[19] C.J. Sung, A. Makino, C.K. Law, Combust. Flame 128 (2002) 422–434.
[20] Z. Chen, M.P. Burke, Y. Ju, Proc. Combust. Inst. 32 (2009) 1253–1260.
[21] Z. Chen, X. Gou, Y. Ju, Combust. Sci. Technol. 182 (2010) 124–142.
[22] J.W. Dold, Combust. Theor. Model. 11 (2007) 909–948.
[23] C.K. Westbrook, Proc. Combust. Inst. 28 (2000) 1563–1577.
[24] A. Linan, F.A. Williams, Fundamental Aspect of Combustion, Oxford University Press, New York, 1993.
[25] A.K. Kapila, J. Eng. Math. 12 (1978) 221–235.
[26] K. Seshadri, N. Peters, Combust. Sci. Technol. 33 (1983) 35–63.
[27] G. Joulin, A. Linan, G.S.S. Ludford, N. Peters, C. Schmidtlaine, SIAM J. Appl. Math. 45 (1985) 420–434.
[28] D.W. Mikolaitis, Combust. Sci. Technol. 49 (1986) 277–288.
[29] R.Y. Tam, Combust. Sci. Technol. 60 (1988) 125–142.
[30] R.Y. Tam, Combust. Sci. Technol. 62 (1988) 297–309.
[31] B.H. Chao, C.K. Law, Int. J. Heat Mass Transfer 37 (1994) 673–680.
[32] J.W. Dold, R.W. Thatcher, A. Omon-Arancibia, J. Redman, Proc. Combust. Inst. 29 (2002) 1519–1526.
[33] J.W. Dold, R.O. Weber, R.W. Thatcher, A.A. Shah, Combust. Theor. Model. 7 (2003) 175–203.
[34] J.W. Dold, R.O. Weber, J. Daou, in: F.J. Higuera, J. Jimenez, J.M. Vega (Eds.), Simplicity, Rigor and Relevance in Fluid Mechanics, Barcelona, Spain, 2004.
[35] V.V. Gubernov, H.S. Sidhu, G.N. Mercer, Combust. Theor. Model. 12 (2008) 407–431.
[36] V.V. Gubernov, H.S. Sidhu, G.N. Mercer, A.V. Kolobov, A.A. Polezhaev, J. Math. Chem. 44 (2008) 816–830.
[37] G. Joulin, P. Clavin, Combust. Flame 35 (1979) 139–153.
[38] P. Clavin, Prog. Energy Combust. Sci. 11 (1985) 1–59.
[39] M.L. Frankel, G.I. Sivashinsky, Combust. Sci. Technol. 40 (1984) 257–268.
[40] C.K. Law, Combustion Physics, Cambridge University Press, 2006.
[41] L. Qiao, Y. Gu, W.J.A. Dam, E.S. Oran, G.M. Faeth, Combust. Flame 151 (2007) 196–208.
[42] L. Qiao, Y. Gan, T. Nishiie, W.J.A. Dam, E.S. Oran, Combust. Flame 157 (2010) 1446–1455.
[43] Z. Chen, X. Qin, B. Xu, Y.G. Ju, F.S. Liu, Proc. Combust. Inst. 31 (2007) 2693–2700.
[44] Z. Chen, Int. J. Hydrogen Energy 34 (2009) 6558–6567.
[45] Z. Chen, M.P. Burke, Y. Ju, Combust. Theor. Model. 13 (2009) 343–364.
[46] Z. Chen, Combust. Flame 157 (2010) 2267–2276.
[47] Z. Chen, Combust. Flame 158 (2011) 291–300.
[48] R.J. Kee, J.F. Grcar, M.D. Smooke, J.A. Miller, Sandia National Laboratory Report SAND85-8240, 1985.
[49] R.J. Kee, F.M. Rupley, J.A. Miller, Sandia National Laboratory Report SAND89-8009B, 1989.
[50] A. Frendi, M. Sibulkin, Combust. Sci. Technol. 73 (1990) 395–413.
[51] J. Li, Z.W. Zhao, A. Kazakov, F.L. Dryer, Int. J. Chem. Kinet. 36 (2004) 566–575.
[52] D. Bradley, P.H. Gaskell, X.J. Gu, Combust. Flame 104 (1996) 176–198.
[53] A.P. Kelley, G. Jomaas, C.K. Law, Combust. Flame 156 (2009) 1006–1013.